3D Simulation of the trap door problem using the Discrete Element Method

Hoang Kien Dang
Department of Civil Engineering and Applied Mechanics – McGill University, Montreal, Quebec, Canada
Mohamed Meguid
Department of Civil Engineering and Applied Mechanics – McGill University, Montreal, Quebec, Canada

ABSTRACT
One of the challenges usually encountered in Discrete Element analysis is the simulation of the initial conditions (e.g. soil density). In this study, an algorithm that has been developed for that purpose is briefly described. A sample with a predefined grain size distribution and density is generated and used to analyze a 3D trap door problem. A scaling technique has been applied to reduce the computational cost associated with 3D modeling. The numerical results are validated using those obtained from physical modeling experiments as well as those reported in the literature.

RÉSUMÉ

La modélisation numérique basée sur la mécanique des milieux continus rencontre de nombreux problèmes liés aux phénomènes de discontinuités (ex. vide au voisinage d'une conduite, problèmes de trappe avec des grands déplacements). Dans cet article, une trappe a été simulée en utilisant la méthode des éléments discrets en trois dimensions. De nombreux effets liés au mouvement de la trappe (ex. déplacement en surface, mécanisme de rupture, phénomène de voûte) ont été examinés. Le comportement macroscopique a également été étudié en utilisant des macro-contraintes équivalentes calculées sur la base des micro-forces de contact. Les résultats sont en accord avec ceux obtenus par modélisations expérimentales ainsi que ceux rapportés dans la littérature.

1 INTRODUCTION

The trapdoor problem has been long used by geotechnical researchers to study the soil behaviour in a wide range of applications such as tunnel design (Terzaghi, 1936), vertical anchors (Meyerhof and Adams, 1968) and embedded pipes (Takagi et al., 1983). Several attempts have been made to develop analytical methods based on experimental observations. Vardoulakis et al. (1981) discussed solutions for the trapdoor force in active and passive modes based on laboratory tests. Vermeer and Sutjiadi (1985) derived a solution for the trapdoor pressure in the passive mode using the available empirical data. Colin (1998) proposed a method to determine the plane strain limit load acting on trapdoor buried in a Mohr-Coulomb soil. An extensive experimental study related to the distribution of earth pressure and surface settlement was carried out by Adachi et al. (2003).

Numerical analyses were also conducted by several researchers to investigate the soil-structure interaction associated with trapdoor problem. Tanaka and Sakai (1993) investigated the progressive failure and scale effects of the trapdoor using an elasto-plastic finite element analysis. The numerical results were also compared with experimental data. Park and Adachi (2002) performed a finite element analysis to study the distribution of earth pressure and the surface settlement profile in a jointed medium.

The analytical and numerical methods mentioned above are based on the concept of continuum mechanics which has proven to work well in most geotechnical applications. However, there are cases where considering the discontinuous nature of the soil is more appropriate such as rockfall and particle flow problems. Since the first discrete element method code was introduced (Cundall and Strack, 1979), it has been used extensively to investigate various engineering problems (e.g. Jensen *et al.*, 1999; Zeghal and Edil, 2002). For the trapdoor problems in particular, formation of shear bands under active/passive conditions was investigated by Murakami et al. (1997) using the 2D discrete element analysis.

In this study, a 3D numerical investigation is conducted to examine the soil movement and earth pressure developing in a typical trap door problem. Emphasis is placed on the realistic simulation of the initial soil conditions using the discrete element method.

2 SIMULATION DETAILS

2.1 Governing equation and force description

This simulation was carried out using the Open Source code YADE (Kozicki and Donze, 2008). The code is designed using dynamic libraries to facilitate the addition of user-defined models. The centered second order finite difference scheme is employed in the software. For this method, the position (orientation) of each particle remains unchanged during each time step; the forces are calculated from the force-displacement relationship. When all forces acting on a particle i, either from other particles or from the boundaries, are known, the problem is reduced to the integration of Newton's equations of motion for the translation and the rotational degrees of freedom

$$m_i \frac{d^2}{dt^2} \vec{r}_i = \vec{f}_i \qquad (1)$$

and

$$I_i \frac{d^2}{dt^2} \overrightarrow{\Phi}_i = \overrightarrow{M}_i \quad (2)$$

where m_i, $\overrightarrow{r}_i$, and $\overrightarrow{\Phi}_i$ are the mass, the vector of position and the vector of orientation in space of particle i, respectively. I_i is the moment of inertia of particle I defined as:

$$I_i = q_i m_i (d_i / 2)^2 \quad (3)$$

where d_i is the diameter of particle i and q_i is the dimensionless shape factor.

Interactions are short range and active on contact only, so that the total force (torque) on particle i is $\overrightarrow{f}_i = \sum_c \overrightarrow{f_i^c}(\overrightarrow{M}_i = \sum_c \overrightarrow{M_i^c})$, where the sum runs over all contacts c of particle i. The torque $\overrightarrow{M_i^c} = \overrightarrow{l_i^c} \times \overrightarrow{f_i^c}$ is related to the force   via the branch vector   from the particle center to the contact point. The damping coefficients are applied to forces and moments for computational purposes. Hence the problems can be solved if all the forces acting on the contact (see Figure 1) are determined. The procedure to calculate the contact force will be discussed in the following.

2.1.1 The contact forces

The contact forces are calculated based on the penalty method which means that the contact forces are evaluated from the overlap volume of two interacting spheres.
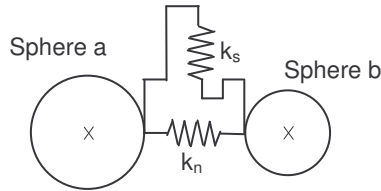

Figure 1. The force-displacement law

2.1.2 The normal force

The normal force is calculated as follow:

$$\overrightarrow{f_{nci}} = \overrightarrow{k_n}\overrightarrow{\delta_n} \quad (4)$$

where $\overrightarrow{f_{nci}}$ is the normal force at contact c on particle i, k_n is the normal stiffness at contact, $\overrightarrow{\delta_n}$ is an relative normal displacement between two particles and $\overrightarrow{n}$ is the branch vector from the contact point to the particle center.

2.1.3 The shear force

The shear force is calculated incrementally using (Hart *et al.* 1988):

$$\Delta \overrightarrow{f_{sci}} = \overrightarrow{k_s} \Delta \overrightarrow{u_t} \quad (5)$$

where $\Delta \overrightarrow{f_{sci}}$ is the incremental shear force, $\overrightarrow{k_s}$ is the tangential stiffness and $\Delta \overrightarrow{u_t}$ is the incremental tangential displacement.

The shear force is truncated if its absolute value is larger than the maximum value given by Mohr–Coulomb criterion:

$$\overrightarrow{f_{sci}^{max}} = \left|\overrightarrow{f_{nci}}\right| \times \tan\phi_i \quad (6)$$

where ϕ_i is the internal friction coefficient.

2.1.4 Macro-micro relationship

The strain energy stored in a given interaction cannot be assumed to be independent of the size of the interacting elements. Therefore interaction stiffnesses are not identical over the sample, but follow a certain distribution depending on the shape and size of the pair of particles interacting. "'Macro-micro'' relations are then needed to derive the local stiffnesses from the macroscopic elastic properties and from the size of the interacting elements. The hypothesis of best fit (Liao *et al.*, 1997; Hentz *et al.*, 2004) is employed to fit the relationship between the Young's modulus E, Poisson's ratio v and the dimensionless value of k_s/k_n:

$$E = \frac{D_{init}^{a,b}}{S_{init}} k_n \frac{\beta + \gamma\beta + \gamma \dfrac{k_s}{k_n}}{\alpha + \gamma \dfrac{k_s}{k_n}} \quad (7)$$

$$v = \frac{1 - \dfrac{k_s}{k_n}}{\alpha + \dfrac{k_s}{k_n}} \quad (8)$$

where $D_{init}^{a,b}$ is the initial distance between two interacting elements a and b, coefficients α, β and γ are the fitted values and S_{init} is an "interaction surface":

$$S_{init} = \pi(\min(R_a, R_b))^2 \quad (9)$$

These relations are simply inverted to obtain the local (micro) stiffnesses at the contacts.

2.2 Macroscopic stress tensor

For an average volume V, the macroscopic stress tensor can be determined as following (Matuttis, 2000)

$$\alpha_{ij} = \frac{1}{V} \sum_{p \in V} \sum_{c=1}^{c} l_i^c f_i^c \tag{10}$$

where f_i^c is the force acting at contact, l_i^c is the branch vector from the particle center to contact point c, indices i and j indicate the Cartesian coordinates. The average volume V should be larger than one particle, thus can contain many contacts. There are two ways to determine if the contact is included into the average volume: the first is that the contact lies within the average volume and the other is that the particle center lies within the average volume. The simplest approach is employed in this paper, i.e. a contact is taken into account if the corresponding particle center lies within the averaging volume. It leads to the fact that two average volumes can have several common contacts. As mentioned by Luding (2004), the stress tensor obtained using this approach underestimates the values obtained with a homogenous shape function covering one particle by less than 1 percent which is considered to be negligible for most engineering applications.

2.3 Stable condition

The specimen is considered to be stable if the ratio of the unbalanced force to the total force is less than a predefined value. In this study, the stability value is taken as 0.01

$$S_c = \frac{\sum |f_i|}{\sum |f_{nci}|} \leq 0.01 \tag{11}$$

where f_i is the resultant force on the body and f_{nci} is the contact force acting at the contact.

2.4 Scheme of the simulation

As shown in **Figure 2**, numerical simulation is carried out on a trapdoor apparatus of the dimensions of 1 m long in the x direction, 0.3 m deep in the z direction and 1 m high in the y direction. The filling material is made of 5,000 monosized particles of approximately 0.026 m in diameter. The height of the fill used in the simulations is 0.42 m. The material properties used in the simulations are given in Table 1.

Table 1 Material properties

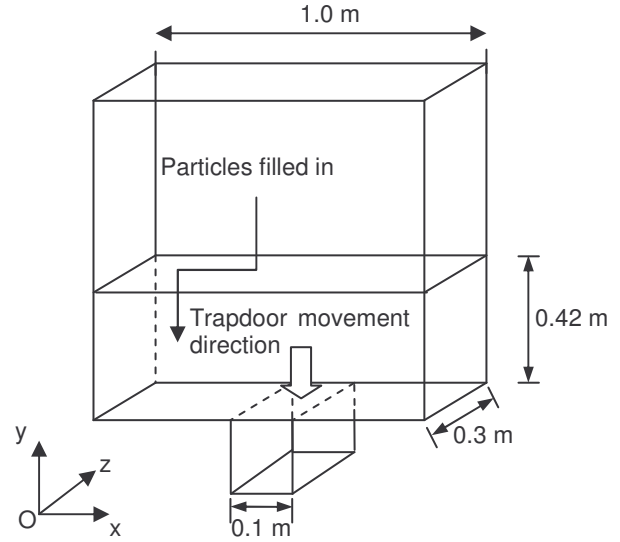| Parameter	Value
Particle density (kg/m^3)	2600
Young's modulus (Pa)	15000000
Poisson's ratio	0.5
Friction degree (degrees)	18
Box's Poisson's ratio	0.2
Box's friction degree	0
Force damping coefficient	0.2
Moment damping coefficient	0.2

Figure 2 Schematic of the trapdoor geometry

As shown in Figure 2, the simulation consists of three stages. Firstly, the initial state is obtained using the gravity packing technique (e.g. pulverization method) often used in laboratory tests. In order to facilitate the visualization of the surface displacement, the surface of the generated specimen is horizontal. Thus the top wall applies a uniform stress σ_{iso} until the specimen reaches the stable condition before the stress is removed. A value of 0.1 m is assigned to the trapdoor width. The trapdoor is allowed to move downward (in the passive direction) in five increments of 0.01 m, 0.05 m, 0.1 m, 0.2 m and 0.4 m. Each increment starts after the previous step reaches the stable condition.

3   RESULTS AND DISCUSSION

3.1 Trapdoor mechanism

To understand the trapdoor mechanism, the force network developing in the area surrounding the trapdoor is shown in Figure 3 for three different values of trapdoor displacements. As the trapdoor moves down a relatively small value (0.01 m), the force network immediately above the trapdoor disappears indicating that a failure zone has developed and the force network above the failure zone became denser and thicker. This is explained by the arching process that lead to the redistribution of pressures in the vicinity of the trapdoor. The shape and direction of the failure zone are similar to those observed in the experiments carried out by Tanaka and Sakai (1993). As the trapdoor translates down to 0.05 m, the stresses carried by the arch increased excessively leading to the destruction of the arch. Consequently, the force network becomes lighter and thinner. The arch destruction process continues as the trapdoor moves further downward. When the trapdoor displacement reaches 0.4 m, the arching phenomena could not be observed anymore.
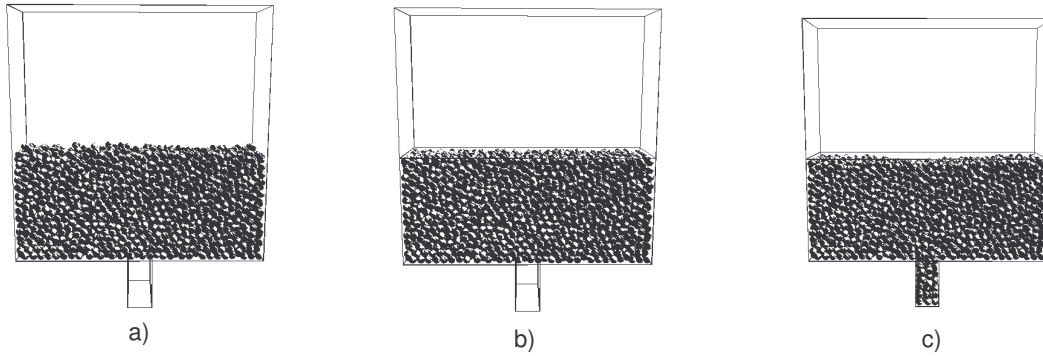
Figure 3 Snapshots of the three stages of simulation: a) initial packing; b) Top wall activated; c) Trapdoor activated
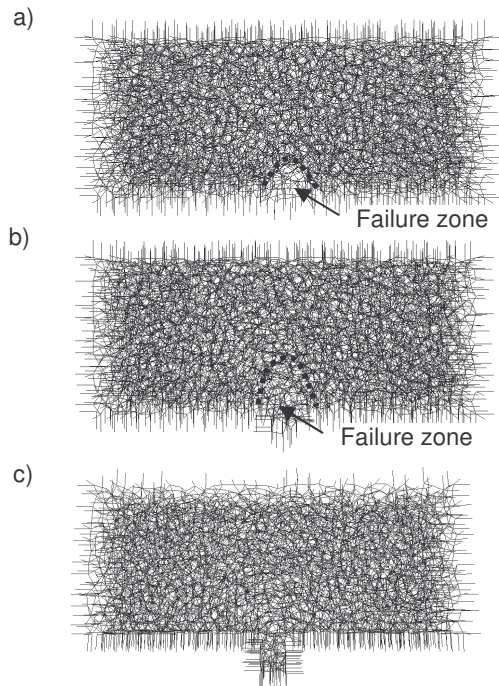

a)

b)

c)

Figure 4 Force network for the different values of trapdoor movement: a) 0.01 m, b) 0.05 m and c) 0.4 m

Figure 5 Variation of average stress on the trapdoor with the trapdoor depth

3.3 Surface displacement

To examine the surface settlement, the positions of the particles on the top of the packing are recorded. Figure 5 shows the positions of the particles along a vertical cross section (@ z = 0.15 m). For trapdoor displacement of less than 0.1 m that corresponds to arching above the trapdoor as indicated above, the surface settlement remains unchanged. At this stage, displacement occurs within the volume immediately above the trapdoor. The soil outside the failure zone is supported by the arch. As the trapdoor displacement increases, the failure zone grows leading arch collapse. Consequently, the surface settlement emerges. By examining Figure 6, the arches start to collapse when the trapdoor displacement reaches a value between 0.1 and 0.2.

3.2 Force acting on the trapdoor

The pressure acting on the trapdoor is calculated by averaging the trapdoor contact forces (see Figure 4). The results are similar to those obtained by Murakami *et al.* (1997). The average stress acting on the trapdoor significantly decreased when the ratio of trapdoor movement to the soil height was relatively small. For trapdoor displacement of 0.05 m, the minimum pressure acting on the trapdoor is found to be approximately 20% of the original value. Further increase in the trapdoor displacement results in an increase in the calculated pressure on the trapdoor.
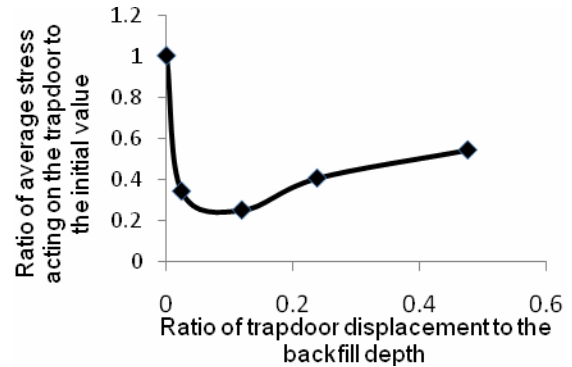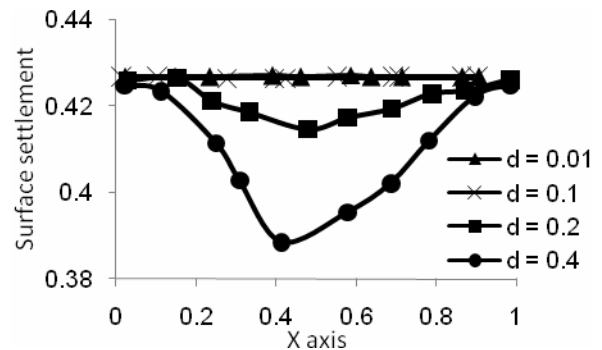

Figure 6 Effect of trapdoor displacement on surface settlement

3.4 Stress distribution

Stresses are calculated using the average volume of a cube of 0.05 m each side. The Von Mises stress distribution for the 0.05 m thick layer (@ z = 0.15 m to 0.2 m) for five different trapdoor displacements are shown in Figure 6. The arching phenomena starts to develop as the trapdoor moves 0.01 m downward, the stress increases significantly in the soil to compensate for the stress carried by the trapdoor. As shown in Figure 6b, the failure zone is expressed by the dark area above the trapdoor position (@ x = 0.45 m, 0.55 m). Increasing the trapdoor movement resulted in increasing the size of the failure zone and decreasing the stresses acting on the arch (Figure 6c). As the trapdoor further moved to 0.1 m, the arch is diminished. This can be explained by the stresses acting on the arches exceeding the arch bearing capacity leading to its destruction. The arches, indicated by the light area immediately above the trapdoor, redevelops as the trapdoor is further displaced (see Figure 6e). Again with further trapdoor displacement (to 0.4 m) the arches completely diminish.
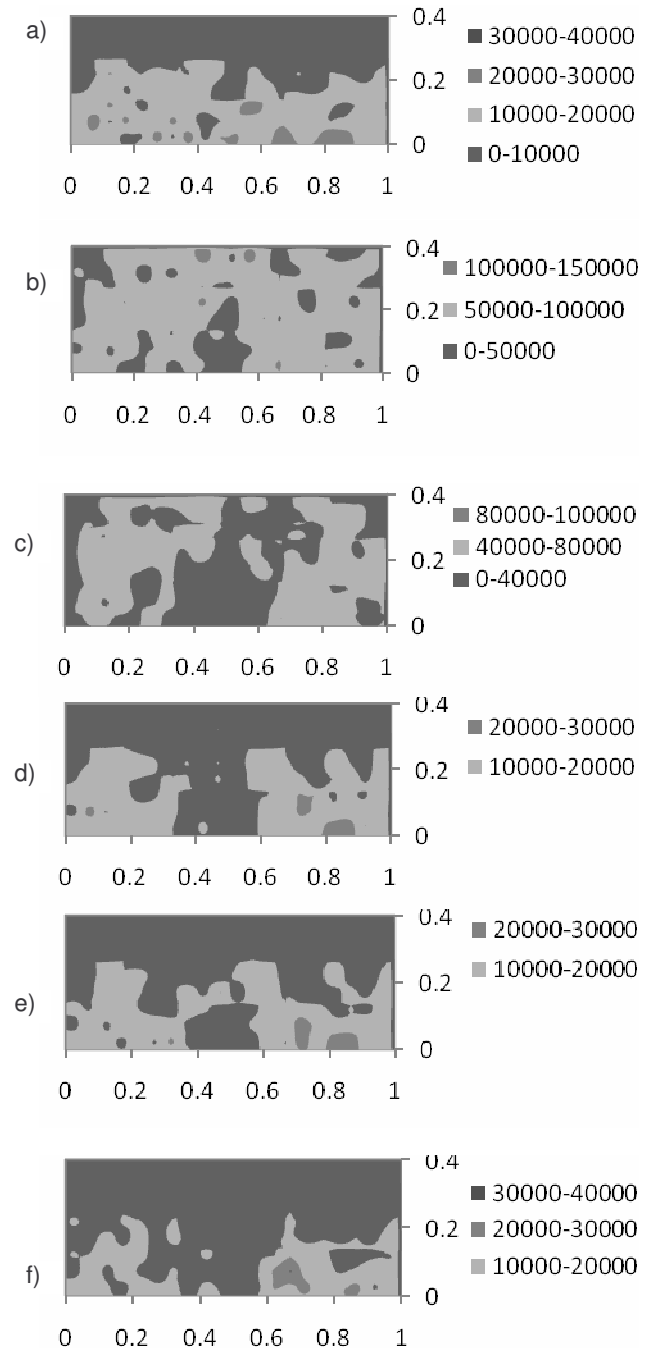

Figure 7 Von Mises stress distributions with different values of trapdoor displacement: a) 0, b) 0.01, c) 0.05, d) 0.1, e) 0.2 and f) 0.4

4   CONCLUSIONS AND IMPLICATIONS

The three-dimensional trapdoor problem was investigated using the discrete element method. The surface displacement and pressure on the trapdoor were calculated and were found to be in good agreement with experimental observations reported in the literature. The simulation allowed for a better understanding of the soil mechanisms associated with continuous trapdoor displacement, such as the arch formation/destruction and the development of local failure zones in the close vicinity of the trapdoor.

References

Adachi, T., M. Kimura and K. Kishida (2003). "Experimental study on the distribution of earth pressure and surface settlement through three-dimensional trapdoor tests." Tunnelling and Underground Space Technology 18(2-3): 171.

Colin, C. S. (1998). "Limit loads for an anchor/trapdoor embedded in an associative coulomb soil." International Journal for Numerical and Analytical Methods in Geomechanics 22(11): 855-865.

Cundall, P. A. and O. D. L. Strack (1979). "A discrete numerical model for granular assemblies." Géotechnique 29(1): 47-65.

Funatsu, T., T. Hoshino, H. Sawae and N. Shimizu "Numerical analysis to better understand the mechanism of the effects of ground supports and reinforcements on the stability of tunnels using the distinct element method." Tunnelling and Underground Space Technology In Press, Corrected Proof.

Jensen, R. P., P. J. Bosscher, M. E. Plesha and T. B. Edil (1999). "DEM simulation of granular media-structure interface: Effects of surface roughness and particle shape." International Journal for Numerical and Analytical Methods in Geomechanics 23(6): 531.

Kozicki, J., F.V. Donze, "Applying an open--source software for numerical simulations using finite element or discrete modelling methods" 2008, Computer Methods in Applied Mechanics and Engineering, (submitted)

Meyerhof, G. G. and J. I. Adams (1968). "The ultimate uplift capacity of foundations." Canadian geotechnical journal 5(4): 225-244.

Murakami, A., H. Sakaguchi and T. Hasegawa (1997). "Dislocation, vortex and couple stress in the formation of shear bands under trap-door problems." Journal of the Japanese Geotechnical Society: Soils and Foundation 37(1): 123-135.

Park, S.-H. and T. Adachi (2002). "Laboratory model tests and FE analyses on tunneling in the unconsolidated ground with inclined layers." Tunnelling and Underground Space Technology 17(2): 181.

Takagi, N., N. Nishio, K. Yoneyama and K. Shimamura (1983). "Development of a strain measurement system for soils and its application to sand around a buried pipe." Soils and Foundations 23(3): 65-79.

Tanaka, T. and T. Sakai (1993). "Progressive failure and scale effect of trap-door problems with granular materials." Soils and Foundations 33(1): 11-22.

Terzaghi, K. V. (1936). Stress distribution in dry and saturated sand above a yielding trap-door. Proceedings of the 1st international conference on soil mechanics and foundation engineering, Cambridge, MA, Harvard University press.

Vardoulakis, I., B. Graf and G., Dudeshus (1981). "Trap-door problem with dry sand: A statical approach based upon model test kinematics." International Journal for Numerical and Analytical Methods in Geomechanics 5(1): 57-78.

Vermeer, P. A. and W. Sutjiadi (1985). The uplift resistance of shallow embedded anchors. Proceedings of 11st international conference on soil mechanics and foundation engineering, San Francisco.

Zeghal, M. and T. B. Edil (2002). "Soil structure interaction analysis: Modeling the interface." Canadian Geotechnical Journal 39(3): 620.